Polarity Dependence of the Radiative and Nonradiative Rates of Flavone Derivatives Comprising Structurally Similar Amino Moieties: Change in the Nature of the Emitting State

Moloy Sarkar, Ravi Kumar Kanaparthi, Bhaswati Bhattacharya, and Anunay Samanta*

School of Chemistry, University of Hyderabad, Hyderabad 500 046, India

Received: October 23, 2007; In Final Form: January 30, 2008

Photophysical behavior of several structurally related electron donor−acceptor flavone derivatives, which have been synthesized and characterized, has been studied as a function of the polarity of the media. Significant variation of the absorption and fluorescence response of the systems has been observed with change in the polarity of the medium. The results show an increase in the radiative rate constant and a decrease in the nonradiative rate constant of the systems with increase in the polarity of the media. This finding has been attributed to the change in the nature of the emitting state from a mixed n−π* and π−π* state to a dominant π−π* state with increase in the polarity of the medium. The results of single-crystal diffraction studies and theoretical calculations based on density functional method support the idea of close proximity of the n−π* and π−π* states and the change in their relative contributions toward the emission process with the polarity of the medium. Laser flash photolysis studies show that the triplet state is not involved in the variation of the fluorescence response of the systems.

1. Introduction

Ever since Sengupta and Kasha reported dual fluorescence of 3-hydroxyflavone (3HF),[1] considerable attention has been paid to this system and its various derivatives by the photophysicists.[2−16] A majority of these studies are focused on the excited-state intramolecular proton transfer (ESIPT) reaction in 3HF, which is responsible for its blue and green fluorescence, attributed respectively to the normal form and the tautomer, the latter produced as a result of ESIPT reaction.[2−9] Specifically, the influence of several extraneous factors such as the polarity, viscosity and hydrogen bond donating ability of the solvents and temperature etc. on the dynamics of ESIPT process and steady-state fluorescence response of the molecule has been investigated in detail.[2−9] While ESIPT is the major theme of research as far as 3HF is concerned, ground state intermolecular proton transfer in the system has also been demonstrated recently.[10,11] Several recent studies have been aimed at exploring the potential applications of the flavone derivatives.[12−16] These include studies on the utility of the systems as fluorescence probes for ratiometric detection of apoptosis,[12] investigation of the antioxidant and antihemolytic effects,[13] probing hydrophobic sites in microheterogeneous systems,[14] and sensing of adenosine-5′-triphosphate[15] and fluoride.[16]

The influence of charge-transfer character on the ESIPT process in 3HF derivatives comprising electron/charge donating moiety has been studied in recent years by Chou and co-workers in an attempt to obtain insight into the proton-transfer coupled electron-transfer reactions in living systems.[17,18] In most cases, the charge-transfer character has been introduced into these systems by substituting the hydrogen atom of the flavones by an amino functionality mostly at C(4′) position. A flavone derivative with an electron donating amino moiety at C(7) position (7-diethylamino-3-methoxyflavone), which has also been studied,[17] shows a higher fluorescence quantum yield with increase in the polarity of the solvents. However, no attention was paid to this observation as excited-state intramolecular charge transfer (ESICT) coupled ESIPT reaction was the focus of this study.

CHART 1

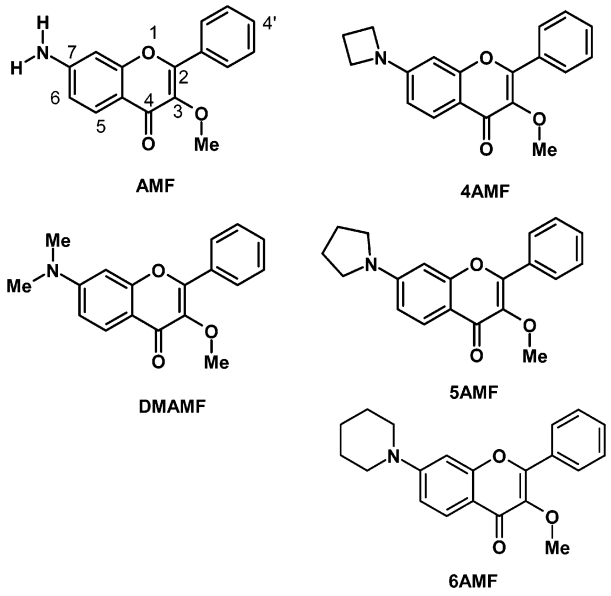

The enhancement of fluorescence efficiency of electron donor−acceptor (EDA) systems in polar environment is somewhat uncommon as most systems of this class exhibit a decrease of the fluorescence efficiency and lifetime and consequent increase of the nonradiative rate constant values with increase in the solvent polarity.[19−21] This observation is attributed

* Corresponding author. E-mail: assc@uohyd.ernet.in.

10.1021/jp710245b CCC: $40.75
Published on Web 03/14/2008

SCHEME 1

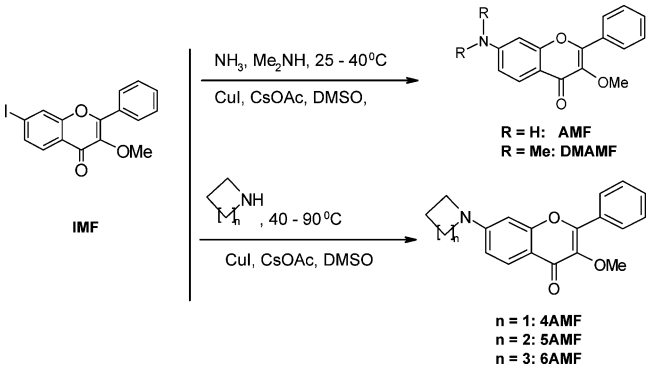

primarily to the fact that EDA systems emit from an intramolecular charge transfer (ICT) state, which is more polar than the ground state. An increase in the polarity of the medium results in a lowering of the S_1-S_0 energy gap due to greater stabilization of the excited-state and consequent increase in the rate of the nonradiative transition to the ground state. An additional factor that often contributes to a further reduction of fluorescence efficiency of a majority of the systems is the internal motion of the amino/dialkylamino moiety or inversion of the amino nitrogen.

We have undertaken this study on a series of 7-amino-3-methoxyflavone derivatives (Chart 1) comprising different amino groups as donor and the carbonyl group of the flavone moiety as acceptor primarily to find out whether all structurally similar 7-amino substituted flavone derivatives show an enhancement of fluorescence efficiency with increase in polarity of the medium and, if this is indeed the case, to find out the reason for this observation. We have chosen the various structurally related amino moieties with a view to examine the influence of the nature of the amino group, if any, on the fluorescence response of the systems. We have used the 3-methoxy derivatives of flavone instead of 3HF to avoid complications from the ESIPT process.

The fluorescence properties of the systems, in particular the fluorescence efficiency, show strong dependence on the polarity of the medium. The results have been interpreted taking into consideration the proximity of two excited states of different symmetries and the change of the nature of the state from a mixed $n-\pi^*$ and $\pi-\pi^*$ state to a pure $\pi-\pi^*$ state with increase in the polarity of the medium. Excited-state calculations of the frontier orbitals based on the TD−DFT method support the experimental data and the above conclusion.

2. Experimental Section

2.1. Materials. 3-Iodophenol, acetyl chloride, cuprous iodide, cesium acetate, benzaldehyde and dimethyl sulfate used for the synthesis of the target compounds were purchased from Acros and used without any further purification. Aqueous solution of ammonia, methylamine and pyrrolidine, piperedine were purchased locally and azetidine was purchased from Acros. All solvents used for spectroscopic measurements (HPLC-grade) were purchased from Merck (Germany) and were distilled and dried by the published procedure.[22] $CDCl_3$ used as solvent for recording the NMR spectra was procured from Merck.

2.2. Synthesis of Methoxyflavone Derivatives. The methoxyflavone derivatives were synthesized in a multistep process. First, 7-iodo-3-methoxy-2-phenyl-chromen-4-one (IMF) was synthesized starting from 3-iodophenol following a procedure

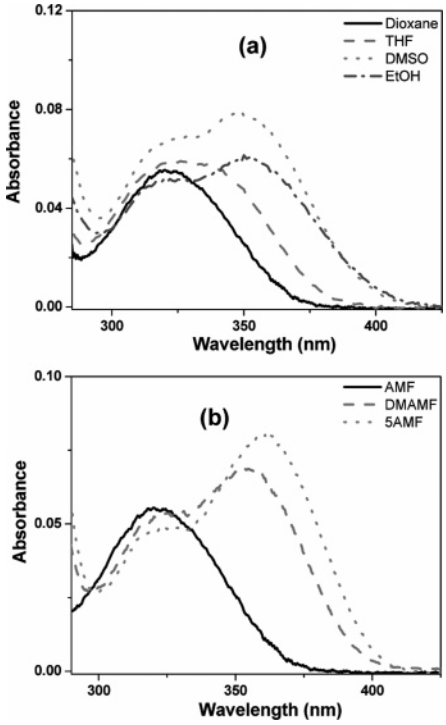

Figure 1. Absorption spectra of (a) **AMF** in some solvents and (b) selected aminomethoxyflavone derivatives in a given solvent, 1,4-dioxane at room temperature.

published elsewhere.[23,24] The amino derivatives were subsequently synthesized from IMF following copper-mediated Ullmann-type reaction (Scheme 1) recently reported by us.[25] The details of the synthetic procedure are as follows.

2.2.1. Acyclic Analogues, AMF and DMAMF. To a stirred mixture of IMF (100 mg, 0.264 mmol), cesium acetate (120 mg, 0.62 mmol), and CuI (5 mol %) in 1.5 mL dry DMSO, dry NH_3 gas (for **AMF**) or Me_2NH (for **DMAMF**) was passed over KOH for 15 min. The dry NH_3 or Me_2NH was generated by adding KOH to an aqueous solution of the respective amines and stirring it for 15 min. The reaction mixture was kept for stirring at room temperature for 24 h under sealed condition after purging N_2 and subsequently heated for another 6 h at 30 °C. The resulting solution was taken up in ethylacetate and washed with brine solution. The organic layer was dried over anhydrous Na_2SO_4, filtered, and concentrated. The crude product was then purified by column chromatography on basic alumina (EtOAc/hexane = 20/80) to give the brown materials.

2.2.2. Cyclic Analogues, 4AMF, 5AMF, and 6AMF. To a solution of IMF (100 mg, 0.264 mmol) in dry DMSO (1.5 mL) the corresponding amine (1.2 mmol) and cesium acetate (120 mg, 0.62 mmol), CuI (5 mol %) were added and the solution was heated to 40−90 °C (depending on the boiling point of the amine) under N_2 atmosphere for 24 h. After being cooled to room temperature, the reaction was quenched with water, extracted with EtOAc (50 mL) and the organic layer was washed with brine solution (100 mL). The organic layer was dried over anhydrous Na_2SO_4 and concentrated through evaporation. The product was purified through column chromatography (basic alumina, EtOAc/hexane = 30/70) as a brown solid.

The compounds were confirmed by following analytical data.

AMF. ^{1}H NMR (400 MHz, $CDCl_3$): δ 8.03−8.05 (m, 3 H), 7.48−7.50 (m, 3 H), 6.67−6.69 (m, 1 H), 6.63 (s, 1 H), 4.26 (s, 2 H), 3.87 (s, 3 H). Anal. Calcd for $C_{16}H_{13}NO_3$: C, 71.90; H, 4.90; N, 5.24. Found: C, 71.83; H, 4.97; N, 5.21. LCMS: *m*/*z* 268 ($M + H^+$).

TABLE 1: Absorption and Emission Spectral Data of the Systems in Various Solvents at Room Temperature

	systems									
	AMF		**DMAMF**		**4AMF**		**5AMF**		**6AMF**	
solvents[a]	λ_{max}^{abs}	λ_{max}^{emis}	λ_{max}^{abs}	λ_{max}^{emis}	λ_{max}^{abs}	λ_{max}^{emis}	λ_{max}^{abs}	λ_{max}^{emis}	λ_{max}^{abs}	λ_{max}^{emis}
toluene (33.9)	324	410	355	435	348	443	360	440	350	442
dioxane (36.0)	324	423	355	450	348	455	360	453	351	455
THF (37.4)	335	442	356	468	349	475	361	472	353	472
EtOAc (38.1)	335	442	353	470	348	476	359	472	349	472
acetone (42.1)	339	457	359	492	352	497	362	495	355	495
ACN (45.6)	340	465	360	502	353	510	365	505	356	510
DMSO (45.1)	350	495	366	525	362	528	371	527	363	526
EtOH (51.9)	352	495	369	520	365	525	375	522	366	525

[a] Quantities in the parenthesis indicate the $E_T(30)$ values of the solvents. $\lambda_{exc} = 350$ nm.

DMAMF. ^{1}H NMR (400 MHz, $CDCl_3$): δ 8.06−8.09 (m, 3 H), 7.48−7.50 (m, 3 H), 6.77 (d, $J = 8.0$ Hz, 1 H), 6.31 (s, 1 H), 3.87 (s, 3 H), 3.10 (s, 6 H). Anal. Calcd for $C_{18}H_{17}NO_3$: C, 73.20; H, 5.80; N, 4.74. Found: C, 73.18; H, 5.87; N, 4.68. LCMS: *m*/*z* 296 ($M + H^+$).

4AMF. ^{1}H NMR (400 MHz, $CDCl_3$): δ 8.05−8.08 (m, 3 H), 7.48−7.50 (m, 3 H), 6.43−6.46 (m, 1 H), 6.26 (s, 1 H), 4.02 (t, $J = 5.4$ Hz, 4 H), 3.87 (s, 3 H), 2.45−2.48 (m, 2 H). Anal. Calcd for $C_{19}H_{17}NO_3$: C, 74.25; H, 5.58; N, 4.56: Found: C, 74.19; H, 5.61; N, 4.53. LCMS: *m*/*z* 308 ($M + H^+$).

5AMF. ^{1}H NMR (400 MHz, $CDCl_3$): δ 8.05−8.09 (m, 3 H), 7.48−7.50 (m, 3 H), 6.63 (d, $J = 8.0$ Hz, 1 H), 6.41 (s, 1 H), 3.87 (s, 3 H), 3.40−3.42 (m, 4 H), 2.06−2.07 (m, 4 H). Anal. Calcd for $C_{20}H_{19}NO_3$: C, 74.75; H, 5.96; N, 4.36. Found: C, 74.71; H, 6.04; N, 4.29. LCMS: *m*/*z* 322 ($M + H^+$).

6AMF. ^{1}H NMR (400 MHz, $CDCl_3$): δ 8.05−8.08 (m, 3 H), 7.48−7.51 (m, 3 H), 6.95−6.97 (m, 1 H), 6.74 (s, 1 H), 3.87 (s, 3 H), 3.39−3.40 (m, 4 H), 1.68−1.69 (m, 4 H), 1.63−1.64 (m, 2 H). Anal. Calcd for $C_{21}H_{21}NO_3$: C, 74.20; H, 6.31; N, 4.18. Found: C, 74.16; H, 6.38; N, 4.12. LCMS: *m*/*z* 336 ($M + H^+$).

2.3. Instrumentation. The absorption and steady-state fluorescence spectra were recorded on UV−Visible spectrophotometer (Cary100, Varian) and spectrofluorimeter (FluoroLog-3, Jobin Yvon), respectively. The fluorescence spectra were corrected for the instrumental response. Time-resolved fluorescence measurements were carried out using a time-correlated single-photon counting (TCSPC) spectrometer (5000, IBH).[26,27] Diode laser ($\lambda_{exc} = 374$ nm, fwhm = 65 ps) was used as the excitation source and an MCP photomultiplier (Hamamatsu R3809U-50) as the detector. The lamp profile was recorded by placing a scatterer (dilute solution of Ludox in water) in place of the sample. Decay curves were analyzed by nonlinear least-squares iteration procedure using IBH DAS6 (Version 2.2) decay analysis software. The transient absorption measurements were performed using a laser flash photolysis setup, which was equipped with a laser system (Q switched Nd:YAG, pulse width = 8 ns) from Spectra Physics (Quanta-Ray INDI series) and a spectrometer from Applied Photophysics (model LKS.60).[28] The spectrometer consisted of a 150 W pulsed xenon lamp, a programmable *f*/3.4 grating monochromator, a digitized oscilloscope (Agilent, 600 MHz), and an R-928 photomultiplier tube. The solutions were excited by the third harmonic (355 nm) of the laser. A perpendicular configuration was chosen for the excitation of the sample. Quartz cuvettes with a path length of 0.3 cm were used. The optical densities of the sample solutions were kept near around 0.1 at the excitation wavelength (355 nm). Applied Photophysics LKS.60 Kinetic spectrometer workstation software was used for the collection and analysis of the data.

The ^{1}H NMR spectra were recorded on a Bruker AVANCE 400 NMR spectrometer at ambient temperature using tetramethylsilane (TMS) as an internal standard. LC mass were recorded on a Shimadzu LCMS-2010A mass spectrometer. Elemental analyses were carried using on a Thermo Finnigan Flash EA 1112 series CHNS analyzer. X-ray data were collected from a Bruker CCD X-ray diffraction system with a graphite-monochromatized Mo Kα radiation ($\lambda = 0.71073$ Å) and the graphics were presented using the crystallographic tool DIAMOND.

2.4. Methods. The fluorescence quantum yields of the system were measured using quinine sulfate as the reference compound ($\Phi_f = 0.546$ in 1 N H_2SO_4).[29] Dilute solutions with OD $\approx$ 0.05 at the excitation wavelength (which typically corresponded to concentrations in the micromolar range) were used for the quantum yield measurements. Optically matched solution solutions of the sample and reference were used for this purpose. The fluorescence spectra for the sample and the reference compound were measured under the same operating conditions and settings. The quantum yields were measured by comparing the areas underneath the fluorescence spectra. All fluorescence spectra were corrected for the instrumental response.

The ground state geometry of the systems were optimized in vacuo using the hybrid DFT functional B3LYP[30,31] at 6-31G* level. Ground state dipole moment was calculated from the optimized structure of the respective system. Excited-state calculations performed within the time-dependent (TD−DFT) framework[32,33] at the B3LYP/6-31G* level in vacuo. The excited-state calculations were also carried out in acetonitrile by self-consistent reaction field (SCRF) method[34] using polarized continuum (PCM) model.[35] All quantum mechanical calculations were performed using the Gaussian 03 program package.[36]

3. Results and Discussions

3.1. Photophysical Behavior. *3.1.1. Absorption.* The UV−vis absorption spectral data of the systems in various solvents covering a wide range of the polarity are collected in Table 1 and representative spectra of some systems illustrating the solvent and amino functionality dependence are shown in Figure 1.

The longest wavelength absorption band of **AMF** shows maximum at 324 nm in toluene. With increase in the polarity of the medium, the band is broadened significantly with buildup of intensity in the long wavelength region (Figure 1). The emergence of a new band with maximum around 350 nm is clearly visible in polar solvents such as dimethyl sulfoxide (DMSO) or ethanol. The absorption maxima of the dialkylated systems are 20−30 nm red-shifted relative to the corresponding maxima of the parent amino system, **AMF**, in any solvent due

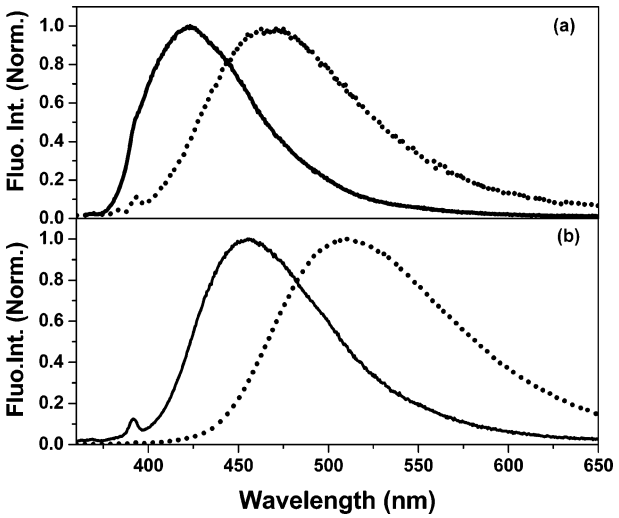

Figure 2. Fluorescence spectra of (a) **AMF** and (b) **5AMF** derivatives in 1,4-dioxane (—) and acetonitrile (···) at room temperature. λ_{exc} = 350 nm.

TABLE 2: Fluorescence Quantum Yields[a] ($\phi_f/10^{-3}$) of the Systems at Room Temperature

	systems (ϕ_f)				
solvents[b]	**AMF**	**DMAMF**	**4AMF**	**5AMF**	**6AMF**
toluene(33.9)	0.5	4.0	4.0	4.0	4.0
dioxane(36.0)	0.5	6.0	6.0	6.0	7.0
THF(37.4)	0.6	19.0	15.0	20.0	24.0
EtOAc(38.1)	1.0	20.0	18.0	26.0	28.0
acetone(42.1)	2.0	61.0	55.0	73.0	72.0
ACN(45.6)	20.0	134.0	151.0	173.0	181.0
DMSO(45.1)	70.0	180.0	190.0	200.0	210.0
EtOH(51.9)	150.0	210.0	220.0	210.0	230.0

[a] ±10%. [b] Quantities in the parenthesis indicate the $E_T(30)$ values of the solvents. λ_{exc} = 350 nm.

to the inductive influence of the alkyl groups. The solvent dependence of the dialkylated derivatives, i.e., the Stokes shift λ_{max}^{abs} with increasing polarity of the medium, is similar to that of the parent system, **AMF**, except that two clearly resolvable peaks are observable for these systems even in less polar medium. The solvent dependent shift of λ_{max}^{abs} is consistent with the dipolar nature of the compound. Among the different dialkylamino systems, not much variation of λ_{max}^{abs} could be observed. It is interesting to note however that the λ_{max}^{abs} values of **5AMF** are relatively red-shifted compared to the other dialkylated systems. That this is due to a more planar amino nitrogen of **5AMF** and consequent increase in the charge conjugation in the molecule is substantiated by the single-crystal X-ray data of two systems, described in section 3.2 and theoretically calculated structure and dipole moment of the systems, presented in section 3.3.

3.1.2. Fluorescence Spectra. Fluorescence spectra of the systems have been recorded in various solvents of different polarity. The wavelengths corresponding to the fluorescence peak positions are collected in Table 1 and some representative spectra are shown in Figure 2.

An increase in the polarity of the medium leads to much more pronounced Stokes shift of the fluorescence maximum (λ_{max}^{em}) compared to the absorption. For example, in the case of **DMAMF**, λ_{max}^{abs} shifts by only 5 nm on changing the solvent from toluene to acetonitrile, whereas λ_{max}^{em} shifts by 67 nm (Table 1). This suggests that the emitting state is more polar than the ground state. The inductive influence of the dialkylamino moieties is also observable in the emission data of the

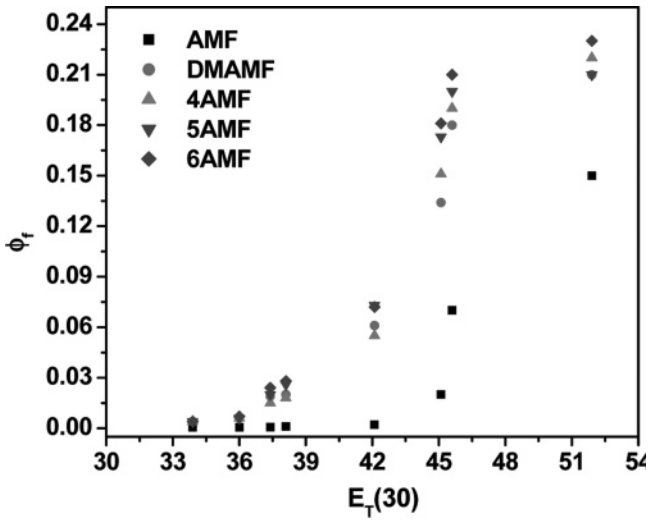

Figure 3. Fluorescence quantum yield of the systems as a function of the $E_T(30)$ value of the solvents. Solvents used here are toluene, 1,4-dioxane, THF, EtOAc, acetone, ACN, DMSO and EtOH with $E_T(30)$ values 33.9, 36.0, 37.4, 38.1, 42.1, 45.6, 45.1, and 51.9, respectively. λ_{exc} = 350 nm.

TABLE 3: Fluorescence Decay Parameters[a] of the Systems in Various Solvents at Room Temperature

	systems				
	AMF	**DMAMF**	**4AMF**	**5AMF**	**6AMF**
solvents	τ_1, τ_2	τ_1, τ_2	τ_1, τ_2	τ_1, τ_2	τ_1, τ_2
toluene	67 (0.95)	60 (0.64)	132 (0.76)	92 (0.83)	98 (0.75)
	910 (0.05)	173 (0.36)	390 (0.24)	230 (0.17)	215 (0.25)
dioxane	50 (0.85)	110 (0.68)	224 (0.96)	95 (0.49)	105 (0.46)
	357 (0.15)	246 (0.32)	1120 (0.04)	236 (0.51)	250 (0.54)
THF	95 (0.96)	257 (0.73)	365 (0.48)	166 (0.34)	110 (0.27)
	587 (0.04)	545 (0.27)	805 (0.52)	463 (0.66)	450 (0.73)
EtOAc	103 (0.85)	270 (0.46)	157 (0.41)	292 (0.45)	315 (0.38)
	485 (0.15)	471 (0.54)	1400 (0.59)	580 (0.55)	600 (0.62)
acetone	70 (0.38)	1390	1890	1650	1790
	272 (0.62)				
ACN	365 (0.91),	3030	3540	3520	3630
	865 (0.09)				
DMSO	1210	3370	3580	3450	3880
EtOH	2270	3330	3250	3150	3170

[a] The fluorescence decays were monitored at the respective fluorescence peak maxima of the compounds. Biexponential fitting was resorted when single-exponential fitting was found unsatisfactory. The fluorescence lifetimes (τ_f) are expressed in ps. The quantities in the parenthesis indicate the relative weight of each component. λ_{exc} = 375 nm.

systems. In any solvent, fluorescence maxima of the dialkylamino systems appear at much longer wavelength region compared to the parent amino analogue (Table 1). Among the different dialkylamino systems, the variation of the λ_{max}^{em} values is found minimal. This includes even **5ANF**, whose absorption behavior is somewhat different from the other systems. The observation led us to suggest that while the planarity of the amino nitrogen or/and dihedral angle between the two ring systems of the various dialkylamino moieties is/are different in the ground state, the amino nitrogen of all the systems is planar in the excited state.

3.1.3. Fluorescence Quantum Yield. The measured fluorescence quantum yields (ϕ_f) of the systems in a series of solvents of different polarity are collected in Table 2. The variation of the ϕ_f values of the systems with the polarity of the medium is highlighted in Figure 3.

In any given solvent, the dialkylamino analogues are found to be more fluorescent compared to the parent system, **AMF**.

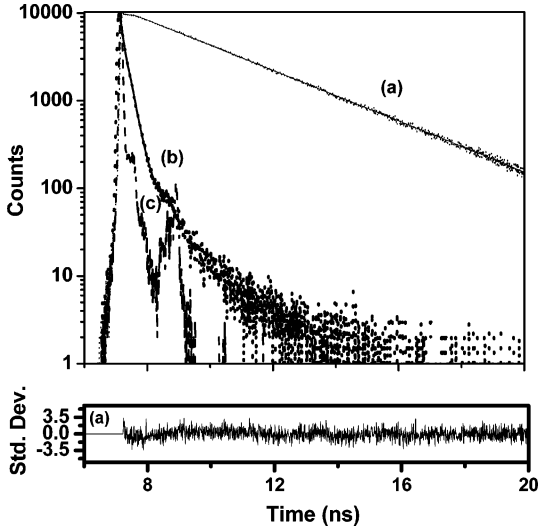

Figure 4. Fluorescence decay curves for **DMAMF** derivative in (a) acetonitrile and (b) 1,4-dioxane. Solutions were excited at 375 nm and emission was monitored at emission maximum. The solid lines represent the best fit to the data. The instrumental response function (lamp profile) is also shown in part c. The weighted deviation is also shown below the decay curves.

TABLE 4: Radiative ($k_r/10^6$ s^{-1}) Rate Constants of the Systems in Various Solvents at Room Temperature

	AMF	DMAMF	4AMF	5AMF	6AMF
toluene	4.5	40.0	21.6	34.7	32.0
dioxane	5.1	38.7	22.6	35.3	37.8
THF	5.3	56.7	24.8	54.8	66.7
EtOAc	6.2	52.6	20.2	57.9	67.0
acetone	10.2	43.9	29.1	44.2	40.2
ACN	26.9	44.2	42.4	49.1	49.9
DMSO	57.9	63.4	53.1	58.0	54.1
EtOH	66.1	63.1	67.7	66.7	72.5

TABLE 5: Nonradiative ($k_{nr}/10^9$ s^{-1}) Rate Constants for the Systems in Various Solvents at Room Temperature

	AMF	DMAMF	4AMF	5AMF	6AMF
toluene	9.1	9.96	5.38	8.66	7.97
dioxane	10.2	6.41	3.75	5.85	5.37
THF	8.8	2.93	1.63	2.70	2.71
EtOAc	6.2	2.59	1.11	2.17	1.98
acetone	5.1	0.67	0.50	0.56	0.52
ACN	1.3	0.28	0.24	0.23	0.22
DMSO	0.8	0.24	0.23	0.23	0.20
EtOH	0.4	0.24	0.24	0.25	0.24

Quantum yields of all the systems increase with increase in the polarity of the solvents. In fact, while changing the solvent from toluene to DMSO, a 140-fold enhancement of the quantum yield value of **AMF** is observed, whereas the other systems show nearly 50-fold enhancement of the quantum yields. This observation is clearly in contrast to the behavior of most other EDA systems which show a significant drop of the fluorescence efficiency with increase in the polarity of the medium.[19−21] As described earlier, this is primarily due to lowering of the energy gap between the ground and ICT emitting state in polar media and consequent enhancement of the nonradiative rate. Hence, the present observation of the enhancement of quantum yields of the system with increase in the polarity of the media is quite interesting.

3.1.4. Fluorescence Decay Behavior. The fluorescence decay parameters of the systems in various solvents are collected in Table 3 and a representative decay profile of **DMAMF** is shown in Figure 4. In less polar media, all the systems show a biexponential decay behavior, whereas in highly polar solvent

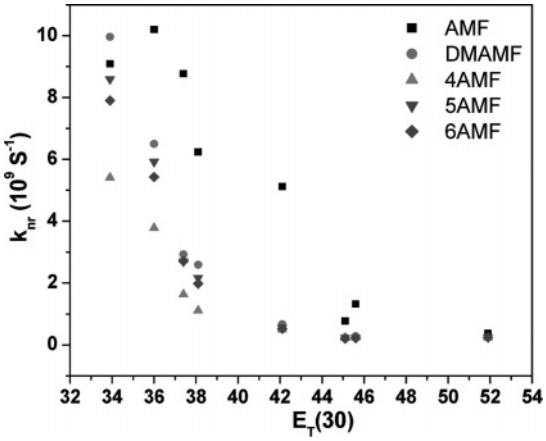

Figure 5. Influence of the polarity of the medium on the nonradiative rate constants of the systems. Solvents used here are toluene, 1,4-dioxane, THF, EtOAc, acetone, ACN, DMSO, and EtOH with E_T (30) values 33.9, 36.0, 37.4, 38.1, 42.1, 45.6, 45.1, and 51.9 respectively. λ_{exc} = 350 nm.

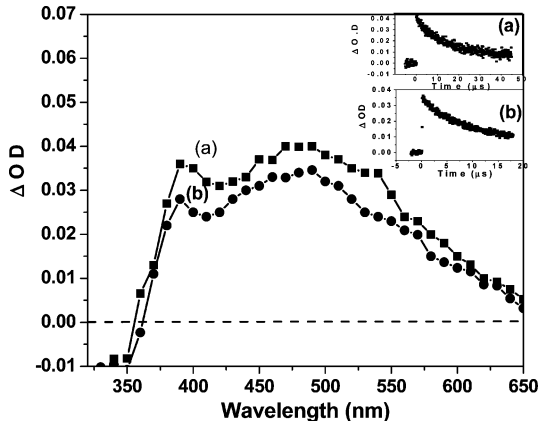

Figure 6. Transient absorption spectra of **AMF** in (a) toluene and (b) acetonitrile. The spectra were obtained 0.5 μs after the laser pulse. Inset shows the decay profile.

a single-exponential decay is observed. A gradual increase in the fluorescence lifetime of the systems is observed with increase in the polarity of the medium. This trend is similar to that observed for the variation of the fluorescence quantum yield with polarity of the solvent. The biexponential nature of the decay profiles of the systems in less polar media is presumably due to the contribution of two nearby states (see later) in the emission process. The single-exponential decay profiles of the systems in highly polar media suggests that the two states are well separated in these media and only one of them is involved in the emission process. In this context, we note that Cheng et al. previously studied the decay profiles of a system similar to those reported here as a function of the polarity of the media and monitoring wavelength.[18] The most striking difference of the results reported by them and the present case is the lack of observation of a short rise time in the decay profiles of our work. This difference is understandable when one takes into account the time resolutions of the two studies. The monitoring wavelength dependence of the decay profiles, in particular the observation of the rise time toward the longer wavelengths, which Cheng et al. reported, is due to an ultrafast excited-state relaxation process that we did not observe because of low time resolution (~40 ps for λ_{exc} = 375 nm) of our setup. However, it is not clear to us why the long-time behavior in the two studies is also somewhat different. Our study of the decay profiles of **DMAMF** in 1,4-dioxane, in which the decay is clearly biexponential, revealed a gradual increase of the weightage of the

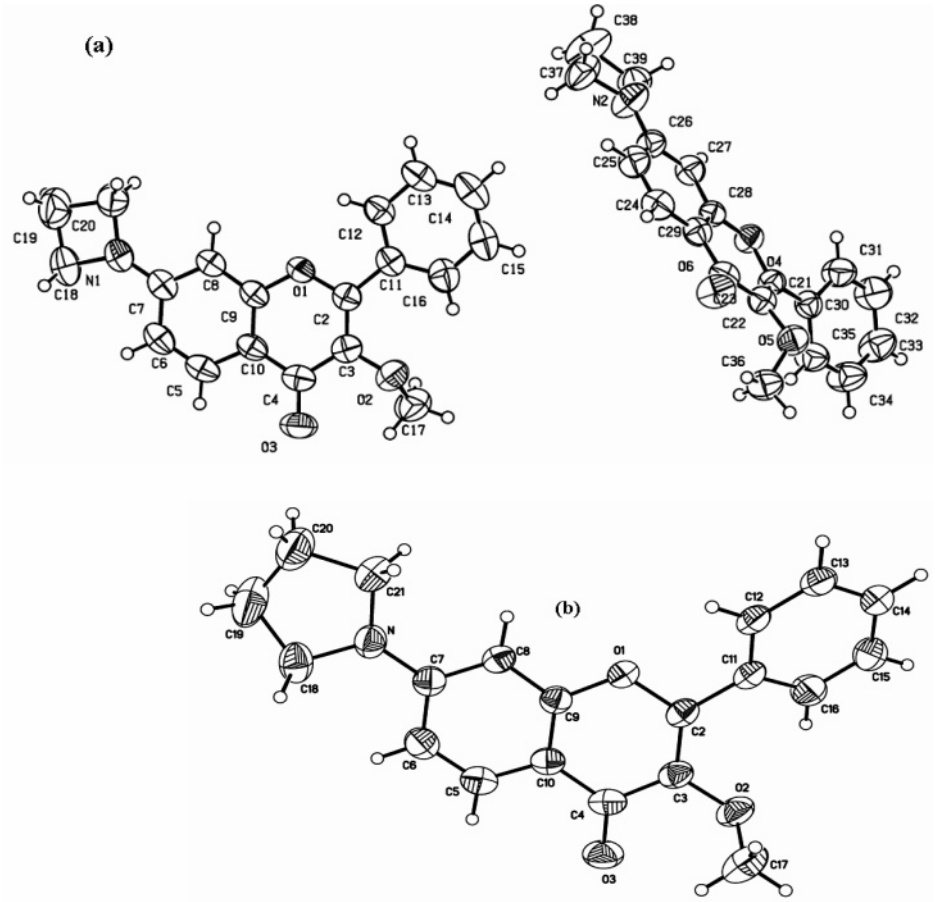

Figure 7. (a) ORTEP diagram of **4AMF** with atoms represented by thermal ellipsoids at 35% probability level, N(1)−C(7) bond length = 1.3459 (3) Å. (b) ORTEP diagram of **5AMF** with atoms represented by thermal ellipsoids at 35% probability level, N−C(7) bond length = 1.3676 (2) Å. CCDC-664794 and 664795 contain the supplementary crystallographic data for this paper. These data can be obtained free of charge from The Cambridge Crystallographic Data Centre via www.ccdc.cam.ac.uk/data_request/cif.

long component with increase in the monitoring wavelength. This observation is consistent with the picture of two different states contributing to the total emission process. The time-resolved behavior has also been studied in mixed solvents of 1.4-dioxane and acetonitrile. As expected, the addition of acetonitrile to a dioxane solution of **DMAMF** results in a gradual (i) shortening of the lifetime and amplitude of the short component and (ii) increase in the lifetime and amplitude of the long component. This trend also substantiates the two-state hypothesis proposed in this manuscript to explain the photophysical data of the systems.

3.1.5. Radiative and Nonradiative Rate Constants. The radiative (k_r) and nonradiative (k_{nr}) rate constants of the systems in different solvents, estimated from the measured values of ϕ_f and τ_f using $k_r = \phi_f/\tau_f$ and $k_{nr} = (1 - \phi_f)/\tau_f$, are collected in Table 4 and Table 5 respectively. For cases with multiexponential decay profiles, the average lifetime values have been used for the calculation of the k_r and k_{nr} values. The variation of the nonradiative rate constants with the polarity of the media is also shown in Figure 5.

As can be seen from Table 4, the radiative rate constants steadily increase with increase in the polarity of the medium for all the systems. This increase is however most prominent for **AMF**, which shows ∼13 times increase in the k_r value upon changing the solvent from toluene to DMSO. The observation suggests that a more allowed state contributes to the emission process with increase in the polarity of the medium. It appears that n−π* and π−π* states of the systems are in close proximity. In nonpolar medium, both the states contribute to the absorption and/or emission process, though they cannot be resolved spectrally. However, the weight of the π−π* state in the emission process is significantly increased in polar medium as enhanced polarity shifts a n−π* state toward higher energy and a π−π* state toward lower energy. This conclusion is consistent with the absorption spectral data of the systems and the observation of 10−15% increase in the molar extinction coefficient values of the first absorption band of the systems.[37] The nonradiative rate constants for all the systems are found to be higher in nonpolar media compared to those in polar media. For example, **AMF** shows a 12 times decrease in the nonradiative rate constant upon changing the solvent from toluene to DMSO (Table 5). A major change of the radiative and nonradiative rate constants of the systems upon changing the polarity of the solvent can be explained considering a change in the nature of the emitting state with change in solvent. In the present case, the results imply that more allowed π−π* state contributes to the emission process in polar media. The proximity effect of the two states, which is reflected in the photophysical behavior of the systems, has been observed earlier in many systems.[38] Further information on this aspect is provided by the results of theoretical calculations, presented in section 3.2.2.

3.1.6. Triplet State Study. In order to determine whether the change of the k_{nr} value of the systems with the polarity of the medium is associated with a corresponding increase/decrease of the triplet yield of the systems, we have investigated the triplet

TABLE 6: Some Structural Parameters[a] of the Systems along with Their Ground State Dipole Moments (μ_g)

	N_1-C_7 bond length		$C_6C_7N_1H$/Cx dihedral angle		bond angles around N_1		
systems	crystal	theory[b]	crystal	theory[b]	crystal	theory[b]	μ_g (D) theory[b]
AMF		1.387		160.04		112.66	4.41
						120.80	
						,119.95	
DMAMF		1.379		175.86		119.31	5.41
						119.70	
						120.27	
4AMF	1.346	1.373	173.10	159.09	95.10	93.95	5.31
					130.88	127.62	
					132.91	127.81	
5AMF	1.368	1.371	179.10	174.69	119.81	112.55	5.94
					123.74	123.48	
					123.85	123.97	
6AMF		1.400		135.84		113.09	4.83
						119.06	
						118.61	

[a] Bond lengths are expressed in Å and bond angles and dihedral angles are in degrees. [b] From B3LYP/6-31G* calculations.

TABLE 7: Lowest Energy Transition (B3LYP/6-31G*) of the Systems

systems	medium	tr. energy (eV)	osc. strength	MOs involved (tr. coeff)	nature
AMF	in vacuo	3.535	0.024	HOMO-2 → LUMO (0.612)	n → π^*
				HOMO → LUMO (−0.279)	$\pi \rightarrow \pi^*$
	acetonitrile	3.552	0.314	HOMO-2 → LUMO (0.136)	n → π^*
				HOMO → LUMO (0.656)	$\pi \rightarrow \pi^*$
DMAMF	in vacuo	3.509	0.110	HOMO-2 → LUMO (0.484)	n → π^*
				HOMO-1 → LUMO (−0.153)	$\pi \rightarrow \pi^*$
				HOMO → LUMO (−0.444)	$\pi \rightarrow \pi^*$
	acetonitrile	3.336	0.302	HOMO → LUMO (−0.675)	$\pi \rightarrow \pi^*$
4AMF	vacuo	3.518	0.086	HOMO-2 → LUMO (0.530)	n → π^*
				HOMO-1 → LUMO (−0.162)	$\pi \rightarrow \pi^*$
				HOMO → LUMO (−0.384)	$\pi \rightarrow \pi^*$
	acetonitrile	3.358	0.323	HOMO → LUMO (0.674)	$\pi \rightarrow \pi^*$
5AMF	vacuo	3.485	0.192	HOMO-2 → LUMO (−0.336)	n → π^*
				HOMO-1 → LUMO (−0.126)	$\pi \rightarrow \pi^*$
				HOMO → LUMO (0.571)	$\pi \rightarrow \pi^*$
	acetonitrile	3.254	0.309	HOMO → LUMO (−0.676)	$\pi \rightarrow \pi^*$
6AMF	vacuo	3.487	0.112	HOMO-2 → LUMO (0.489)	n → π^*
				HOMO-1 → LUMO (−0.154)	$\pi \rightarrow \pi^*$
				HOMO → LUMO (0.439)	$\pi \rightarrow \pi^*$
	acetonitrile	3.311	0.306	HOMO → LUMO (0.677)	$\pi \rightarrow \pi^*$

state of **AMF** in toluene and acetonitrile using time-resolved transient absorption technique. Laser flash photolysis (λ_{exc} = 355 nm) of **AMF** shows a broad transient absorption band in the 350−650 nm region in both the solvents. Considering the facts that (i) bubbling of O_2 or air leads to the disappearance/diminishing intensity of the band and (ii) long lifetime (8 μs in toluene and 12 μs in acetonitrile) of the transient, this absorption can be attributed to triplet−triplet transition of **AMF**. This assignment is also supported by the literature data of a similar derivative.[39] While the fluorescence quantum yield of **AMF** in toluene is lower than that in acetonitrile by a factor of 40, we find that the end-of-pulse absorption change yields $(\Delta OD)_0$ values for optically matched solutions of **AMF** in two solvents of different polarity that are nearly identical (Figure 6).

Assuming that the molar extinction coefficients for the T−T absorption are very similar in the two solvents,[40] the results imply that the triplet yield of the system is very similar in the two solvents. Thus, the decrease of the nonradiative rate constants with increase in the polarity of the media is not due to any change of the intersystem crossing efficiency of the systems. Obviously, the efficiency of the internal conversion process is affected as the polarity of the media is changed.

3.2. Crystal Structures. Two systems, **4AMF** and **5AMF**, for which good single crystals could be obtained (from chloroform), have been characterized by single-crystal X-ray diffraction studies.[41] The ORTEP diagrams of the systems are shown in Figure 7. The structural parameters useful for an understanding of the photophysics of these systems are the N_1−C_7 bond length, angles around the amino nitrogen and dihedral angle between the planes containing the amino functionality and flavone moiety. These quantities, which are listed in Table 6, indicate the extent of electronic conjugation between the two rings and the planarity of the amino nitrogen. The values clearly suggest a more planar nature of the amino nitrogen of **5AMF**.

3.3. Theoretical Calculations. *3.3.1. Ground State Calculations.* The ground state geometries of the systems have been optimized in vacuo at B3LYP/6-31G* level. Some important geometrical parameters of the optimized structures are collected in Table 6. The results suggest that the amine functionalities are twisted with respect to the flavone ring and the twist angles are different for different systems. The calculated ground state dipole moments of all the systems, which vary between 4.41 and 5.94 D, are also listed in this table. The data suggests that among all the systems **5AMF**, which comprises the most planar nitrogen atom, is the most dipolar molecule. **DMAMF** is second most polar system and **AMF** is the least polar system. A higher moment of the dialkylated systems compared to **AMF** is consistent with the inductive influence of the alkyl groups. The

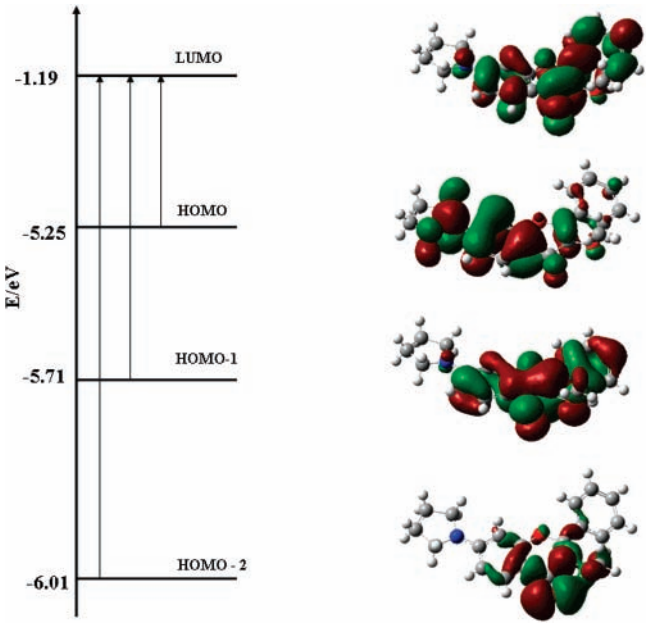

Figure 8. Molecular orbital picture associated with the first excited-state of **5AMF** in the gas phase. The oribitals were obtained by TD−DFT method at B3LYP/6-31G* level.

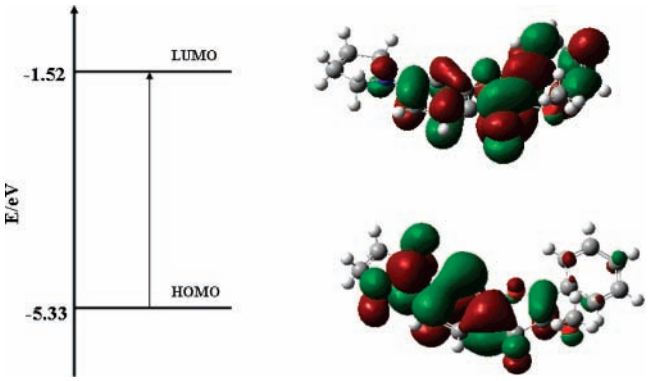

Figure 9. Molecular orbital picture associated with the first excited-state of **5AMF** in acetonitrile. The oribitals were obtained by TD−DFT method at the 6-31G* level via SCRF/PCM solvation scheme.

variation of the dipole moment among the different dialkylated systems is due to the difference in the planarity of the amino nitrogen and the dihedral angle indicated in the table.

3.3.2. Excited State Calculations. We have theoretically studied the energetics of different molecular orbitals associated with the lowest excited-state of the systems to find out whether the increase in the fluorescence efficiency on changing the medium from a nonpolar to a polar one is associated with a change in the nature of the emitting state. Excited-state calculations (TD−DFT, B3LYP/6-31G* level) have been performed in the gas phase as well as in acetonitrile, the latter by self-consistent reaction field (SCRF) method using the polarized continuum (PCM) model. The representative molecular orbital pictures associated with the first excited-state for **5AMF** in the gas phase and in acetonitrile are shown in Figure 8 and Figure 9 respectively.

The excitation energy for the lowest energy transition, the nature of this transition obtained by careful examination of the orbitals involved in the transition and the oscillator strength of the transition are collected in Table 7. The calculated excitation energies of the systems agrees reasonably well with the experimentally determined quantities. As for example, the calculated lowest energy transition of **DMAMF** is found to be at 3.51 eV in vacuo and the experimental energy estimated from the λ_{max}^{abs} value in toluene is 3.49 eV. The calculations show that three different excitations, HOMO−LUMO, (HOMO-1)−LUMO and (HOMO-2)−LUMO contribute to the first excited-state of the systems in vacuum. The HOMO−LUMO, (HOMO-1)−LUMO and (HOMO-2)−LUMO excitations, as determined from the shapes of the molecular orbitals, are assigned to $\pi-\pi^*$, $\pi-\pi^*$, and $n-\pi^*$ transitions. While three different excitations correspond to the first excited-state in the gas phase, the contribution of the (HOMO-2)−LUMO excitation, an $n-\pi^*$ transition, is clearly the largest (*vide* Table 7). Interestingly, in polar medium (such as acetonitrile), the excitation mainly arises from the HOMO−LUMO excitation, having $\pi-\pi^*$ character of the transition (*vide* Table 7). However, for **AMF** a minor contribution arises from (HOMO-2)−LUMO excitation, with $n-\pi^*$ character, remains. The results clearly suggest that in the gas-phase both $n-\pi^*$ and $\pi-\pi^*$ states contribute to the photophysical response of the systems with the major contribution arising from the $n-\pi^*$ state. The results also show that the first excited-state is of $\pi-\pi^*$ in nature in acetonitrile. These results are consistent with the previous optical and magnetic resonance studies establishing that the $n-\pi^*$ and $\pi-\pi^*$ states of the flavones are strongly mixed.[42] Theoretical results indicate clearly that a large contribution due to the $n-\pi^*$ character of the first excited-state is primarily responsible for relatively low radiative efficiency of the systems in nonpolar media. However, the $\pi-\pi^*$ state, which becomes the lowest excited-state in polar media, is responsible for enhanced radiative efficiency in these media.

4. Conclusion

This study on several structurally related 7-amino/dialkylamino flavone derivatives reveals that the photophysical behavior of these systems differs from that of a majority of conventional EDA molecules. The most notable difference is the proximity of the multiple excited states and its direct influence on the fluorescence behavior of the flavones. While the emission behavior of commonly encountered EDA systems is usually dictated by low-lying intramolecular charge transfer state and a decrease in fluorescence efficiency with increase in the polarity of the medium is commonly observed, the amino flavones show enhanced fluorescence efficiency in polar medium. No influence of the internal motion of the amino moieties on the fluorescence response of the systems is observed. The laser flash photolysis measurements show that the intersystem crossing efficiency in the systems is not influenced by the polarity of the medium. The theoretical calculations confirm that the emitting state in these flavones is of mixed $n-\pi^*$ and $\pi-\pi^*$ nature in nonpolar medium. In polar medium, the separation between the two states is enhanced and the $\pi-\pi^*$ state becomes the lowest excited-state responsible for enhanced emission of the systems.

Acknowledgment. This work is supported by the Ramana Fellowship of the Department of Science and Technology (DST), Government of India and the UPE Program of the University Grants Commission (UGC). The X-ray structure determination was performed at the National Single-Crystal Diffractometer Facility (funded by the DST) of the School of Chemistry, University of Hyderabad. M.S. and B.B. thank the Council of Scientific and Industrial Research (CSIR) and R.K.K. thanks the UGC for fellowships.

Supporting Information Available: Table S1, molar extinction coefficient values of the systems in two different solvents, and Table S2, data collections and structure refinement details of crystal structures of **4AMF** and **5AMF**. This material is available free of charge via the Internet at http://pubs.acs.org.

References and Notes

(1) Sengupta, P. K.; Kasha, M. *Chem. Phys. Lett.* **1979**, *68*, 382.
(2) McMorrow, D.; Kasha, M. *J. Am. Chem. Soc.* **1983**, *105*, 5133.
(3) Kasha, M. *J. Chem. Soc., Faraday Trans. 2* **1986**, *82*, 2379.
(4) Dennison, S. M.; Guharay, J.; Sengupta, P. K. *Spectrochim. Acta, Part A* **1999**, *55*, 903.
(5) Ameer-Beg, S.; Ormson, S. M.; Brown, R. G.; Matousek, P.; Towrie, M.; Nibbering, E. T. J.; Foggi, P.; Neuwahl, F. V. R. *J. Phys. Chem. A* **2001**, *105*, 3709.
(6) Klymchenko, A. S.; Pivovarenko, V. G.; Demchenko, A. P. *J. Phys. Chem. A* **2003**, *107*, 4211.
(7) Chattopadhyay, N.; Barroso, M.; Serpa, C.; Arnaut, L. G.; Formosinho, S. J. *Chem. Phys. Lett.* **2004**, *387*, 258.
(8) Oncul, S.; Demchenko, A. P. *Spectrochim. Acta, Part A* **2006**, *65*, 179.
(9) Tomin, V. I.; Jaworski, R. *Eur. Phys. J.: Spec. Top.* **2007**, *144*, 123.
(10) Mandal, P. K.; Samanta, A. *J. Phys. Chem. A* **2003**, *107*, 6334.
(11) Shyamala, T.; Mishra, A. K. *Photochem. Photobiol.* **2004**, *80*, 309.
(12) Shynkar, V. V.; Klymchenko, A. S.; Kunzelmann, C.; Duportail, G.; Muller, C. D.; Demchenko, A. P.; Freyssinet, J. M.; Mély, Y. *J. Am. Chem. Soc.* **2007**, *129*, 2187.
(13) Chaudhuri, S.; Banerjee, A.; Basu, K.; Sengupta, B.; Sengupta, P. K. *Int. J. Biol. Macromol.* **2007**, *41*, 42.
(14) Ozturk, T.; Klymchenko, A. S.; Capan, A.; Oncul, S.; Cikrikci, S.; Taskiran, S.; Tasan, B.; Kaynak, F. B.; Ozbey, S.; Demchenko, A. P. *Tetrahedron* **2007**, *63*, 10290.
(15) Yushchenko, D. A.; Vadzyuk, O. B.; Kosterin, S. O.; Duportail, G.; Mély, Y.; Pivovarenko, V. G. *Anal. Biochem.* **2007**, *369*, 218.
(16) Sakar, M.; Samanta, A. *J. Phys. Chem. B* **2007**, *111*, 7027.
(17) Chou, P. T.; Huang, C. H.; Pu, S. C.; Cheng, Y. M.; Liu, Y. H.; Wang, Y.; Chen, C. T. *J. Phys. Chem. A* **2004**, 6452.
(18) Cheng, Y. M.; Pu, S. C.; Yu, Y. C.; Chou, P. T.; Huang, C. H.; Chen, C. T. *J. Phys. Chem. A* **2005**, *109*, 11696.
(19) Soujanya, T.; Fessenden, R. W.; Samanta, A. *J. Phys. Chem.* **1996**, *100*, 3507.
(20) Saha, S.; Samanta, A. *J. Phys. Chem. A* **1998**, *102*, 7903.
(21) Saha, S.; Samanta, A. *J. Phys. Chem. A* **2002**, *106*, 4763.
(22) Perrin, D. D.; Armerego, W. L. F.; Perrin, D. R. *Purification of Laboratory Chemicals*; Pergamon Press: New York, 1980.
(23) Ormson, S. M.; Brown, R. G.; Vollmer, F.; Rettig, W. *J. Photochem. Photobiol. A: Chem.* **1994**, *81*, 65.
(24) Meyer, N. D.; Haemers, A.; Mishra, L.; Pandey, H.; Pieters, L. A. C.; Dirk, A.; Berghe, V.; Vlietinck, A. J. *J. Med. Chem.* **1991**, *34*, 736.
(25) Sarkar, M.; Samanta, A. *Synthesis* **2006**, *20*, 3425.
(26) Paul, A.; Samanta, A. *J. Phys. Chem. B* **2007**, *111*, 4724.
(27) Paul, A.; Samanta, A. *J. Phys. Chem. B* **2007**, *111*, 1957.
(28) Bhattacharya, B.; Samanta, A. *Chem. Phys. Lett.* **2007**, *442*, 316.
(29) Demas, J. N.; Crosby, G. A. *J. Phys. Chem.* **1971**, *75*, 991.
(30) Lee, C.; Yang, W.; Parr, R. G. *Phys. Rev. B* **1988**, *37*, 785.
(31) Becke, D. A. *J. Chem. Phys.* **1993**, *98*, 5648.
(32) Bauernschmitt, R.; Ahlrichs, R. *Chem. Phys. Lett.* **1996**, *256*, 454.
(33) Casida, M. E.; Jamorski, C.; Casida, K. C.; Salahub, D. R. *J. Chem. Phys.* **1998**, *108*, 4439.
(34) Wong, M. W.; Frish, M. J.; Weiberg, K. B. *J. Am. Chem. Soc.* **1991**, *113*, 4776.
(35) Cossi, M.; Barone, V. *J. Chem. Phys.* **2000**, *112*, 2427.
(36) Frisch, M. J. Trucks, G. W.; Schlegel, H. B.; Scuseria, G. E.; Robb, M. A.; Cheeseman, J. R.; Zakrzewski, V. G.; Montgomery, J. A., Jr.; Stratmann, R. E.; Burant, J. C.; Dapprich, S.; Millam, J. M.; Daniels, A. D.; Kudin, K. N.; Strain, M. C.; Farkas, O.; Tomasi, J.; Barone, V.; Cossi, M.; Cammi, R.; Mennucci, B.; Pomelli, C.; Adamo, C.; Clifford, S.; Ochterski, J.; Petersson, G. A.; Ayala, P. Y.; Cui, Q.; Morokuma, K.; Malick, D. K.; Rabuck, A. D.; Raghavachari, K.; Foresman, J. B.; Cioslowski, J.; Ortiz, J. V.; Stefanov, B. B.; Liu, G.; Liashenko, A.; Piskorz, P.; Komaromi, I.; Gomperts, R.; Martin, R. L.; Fox, D. J.; Keith, T.; Al-Laham, M. A.; Peng, C. Y.; Nanayakkara, A.; Gonzalez, C.; Challacombe, M.; Gill, P. M. W.; Johnson, B.; Chen, W.; Wong, M. W.; Andres, J. L.; Gonzalez, C.; Head-Gordon, M.; Replogle, E. S; Pople, J. A. Gaussian 98. Gaussian, Inc: Pittsburgh, PA, 1998.
(37) Molar absorption coefficient values of the systems in toluene and acetonitrile are provided in the supporting information.
(38) See for example: de Melo, J. S.; Becker, R. S.; Elisel, F.; Macanita, A. L. *J. Chem. Phys.* **1997**, *107*, 6062.
(39) Christoff, M.; Toscano, V. G.; Badder, W. J. *J. Photochem. Photobiol. A: Chem.* **1996**, *101*, 11.
(40) Carmichael, I.; Hug, G. L. *J. Phys. Chem. Ref. Data* **1986**, *15*, 1.
(41) Essential crystallographic data are provided in the supporting information.
(42) Gallivan, J. B.; Brinen, J. S. *Chem. Phys. Lett.* **1971**, *10*, 455.